Eur. Phys. J. E **10**, 45–54 (2003)
DOI: 10.1140/epje/e2003-00001-6

THE EUROPEAN PHYSICAL JOURNAL E

Phase behavior and structure of an ABC triblock copolymer dissolved in selective solvent

N.P. Shusharina[1], P. Alexandridis[1,a], P. Linse[2], S. Balijepalli[3], and H.J.M. Gruenbauer[4]

[1] Department of Chemical Engineering, University at Buffalo, The State University of New York, Buffalo, NY 14260-4200, USA
[2] Physical Chemistry 1, Center for Chemistry and Chemical Engineering, Lund University, P.O. Box 124, S-221 00 Lund, Sweden
[3] New Product & Mathematical Modeling Group, Corporate R&D, The Dow Chemical Co., Midland, MI 48674, USA
[4] New Business Development, Dow Benelux N.V., 4530 AA Terneuzen, The Netherlands

Received 17 April 2002
Published online: 21 January 2003 – © EDP Sciences, Società Italiana di Fisica, Springer-Verlag 2003

Abstract. A mean-field lattice theory is applied to predict the self-assembly into ordered structures of an ABC triblock copolymer in selective solvent. More specifically, the composition-temperature phase diagram has been constructed for the system $(C)_{14}(PO)_{12}(EO)_{17}$/water, where C stands for methylene, PO for propylene oxide and EO for ethylene oxide. The model predicts thermotropic phase transitions between the ordered hexagonal, lamellar, reverse hexagonal, and reverse cubic phases, as well as the disordered phase. The thermotropic behavior is a result of the temperature dependence of water interaction with EO- and PO-segments. The lyotropic effect (caused by changing the solvent concentration) on the formation of different structures has been found weak. The structure in the ordered phases is described by analyzing the species volume fraction profiles and the end segment and junction distributions. A "triple-layer" structure has been found for each of the ordered phases, with each layer rich in C-, PO-, and EO-segments, respectively. The blocks forming the layers are not stretched. The dependence of the domain spacing on polymer volume fraction and temperature is also considered.

PACS. 36.20.-r Macromolecules and polymer molecules – 64.75.+g Solubility, segregation, and mixing; phase separation – 61.20.Gy Theory and models of liquid structure – 07.05.Tp Computer modeling and simulation

1 Introduction

Segregation in block copolymer systems leads to interesting self-assembling properties and finds a number of applications [1,2]. Due to block incompatibility, block copolymer molecules form assemblies, spherical or cylindrical micelles, or planar lamellae, which are characterized by segregated internal structure. Particularly, one can distinguish nano-domains rich with segments belonging to different blocks. Spherical and cylindrical micelles can organize into ordered phases, cubic and hexagonal, respectively; planar aggregates form lamellar phases. Single-component block copolymer systems (melts) can undergo phase transitions while the temperature and/or the block composition in the system change. Since the early work of Leibler [3], the theory of diblock copolymer melts has been developed by many authors [4–6]. The variety of liquid crystalline phases in molten diblock copolymers with two incompatible blocks has been extensively studied using different experimental methods [7–10].

The introduction of selective solvent into a block copolymer melt renormalizes the direct segment-segment interaction. The incompatibility of the blocks is enhanced due to their different affinity to the solvent. Polarity or solubility of the segments are the factors which determine an internal domain structure. Phase transitions among different morphologies in block copolymer systems in the presence of selective solvent are caused by varying the polymer/solvent ratio or temperature. Recent studies demonstrate a growing interest in the phase behavior of block copolymers in selective solvents [11–15].

Poly(ethylene oxide-*b*-propylene oxide-*b*-ethylene oxide), $(EO)_m(PO)_n(EO)_m$ block copolymers, commercially available as Pluronics or Poloxamers, in water (selective solvent) are systems that exhibit a remarkable structural polymorphism [11–13,16–19]. A mean-field lattice theory had been found successful in predicting composition-temperature phase diagrams for PEO/PPO homopolymers and block copolymers in water [20–22]. The calculated phase diagrams were found to be in good agreement with experimentally determined phase diagrams [11,20,23].

[a] e-mail: palexand@eng.buffalo.edu

ABC triblock copolymers are promising because an increased interaction spectrum obviously leads to a richer variety of structures [24–27]. The solution properties of ABC triblock copolymers with different solvophobicity of the blocks have been studied by very few groups [28–30]. Depending on the conditions chosen, aggregates of different morphologies have been found. It is not trivial to obtain the phase diagram of ABC triblock copolymers in selective solvent experimentally because of the large number of parameters defining the phase window. The phase behavior of systems with reduced set of interaction parameters, namely ABC block copolymers mixed with A and C homopolymers [31], and mixture of symmetric AB diblock and ABC triblock copolymer [32], has been investigated. Theoretical investigations of morphologies in ABC block copolymer melts (in the absence of any solvent) have been recently performed [33–38]. However, the phase behavior of ABC-type block copolymers in solution has not been considered.

In the present study we predict the phase behavior of an ABC triblock copolymer $(C)_k(PO)_n(EO)_m$ in the presence of selective solvent (water) on the basis of the mean-field lattice theory used in references [20–22]. The composition of the considered block copolymer molecules determines their self-assembling properties and the influence of external parameters, such as temperature and polymer concentration, on domain organization. Microphase segregation in the system is caused by the significantly different affinity of the blocks to the solvent, and the relative length of the blocks. Since EO and PO exhibit clouding in water at high temperature (lower critical solution temperature), one should expect a significant temperature effect on the hydrophilic/hydrophobic balance. The alkyl block $(C)_k$ is known as highly hydrophobic and its hydrophobicity does not depend strongly on temperature. The difference in hydrophobicity between $(PO)_n$ and $(EO)_m$ blocks is moderate (both of them can be considered as hydrophilic relatively to the $(C)_k$ block), nevertheless, it is known that PEO/PPO block copolymers form microsegregated structures in aqueous solution at sufficiently low temperatures [11,12,23]. Therefore, the combination of $(C)_k$, $(PO)_n$, and $(EO)_m$ in a block copolymer molecule is expected to lead to interesting composition-temperature phase behavior and structure in water.

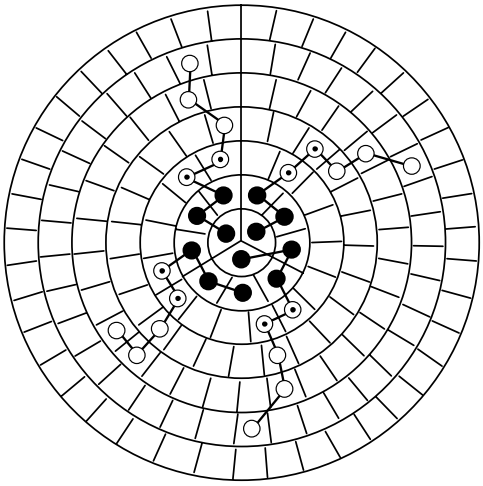

Fig. 1. Two-dimensional illustration of a spherical lattice or a perpendicular cut of a cylindrical lattice with an assembly formed by four triblock copolymers $A_3B_2C_3$ in solvent. The solvophobic segments (filled circles) form the central part of the assembly, whereas the more solvophilic segments (connected open and dot-centered circles) form the outer layer of the assembly. Note the small number of unfavorable contacts between the solvophobic segments and the solvent (unfilled lattice cells).

2 Theoretical modeling

2.1 SCF method

The theory that we use in this work is based on a mean-field lattice model initially developed by Scheutjens and Fleer [39] for describing polymer adsorption from solution. Further extensions of the original theory have been done in several directions. Significant developments deal with a description of polymer chain to treat chain stiffness [40], steric hindrance of the C-C bond [41], and polyelectrolyte effects [42].

As mentioned in the introduction, EO- and PO-containing polymers exhibit a reduced solubility in water at elevated temperature. Above a certain temperature the polymer solution separates into two phases, one polymer rich and one polymer poor. To model the lower consolute point in the binary polymer-solvent systems, an approach suggested by Karlström has been employed [43]. This approach states that the conformations of EO- and PO-segments vary with temperature, and different conformations interact unequally with the surrounding. Quantum mechanics calculations [44] show that the conformations can be divided into two classes or states: one being polar, P, and one being less polar or apolar, AP. The internal energy of the polar states is lower, but their degeneration is low; the apolar states have higher internal energy, but are more degenerated. An extension of the mean-field lattice theory for the case where polymer segments may possess internal degrees of freedom (states) has been reported in [45,46].

More recently, the theory has been applied for predicting composition-temperature phase diagrams for block copolymers in selective solvent [21,22]. In the latest approach the free energies of disordered micelle-free and micelle-containing solutions and of different ordered phases as a function of the composition and temperature were used for the determination of the phase boundaries. Each ordered phase has a structure unit, which in the following is referred to as a domain, of a certain symmetry.

A complete theoretical description of the model is presented in reference [46]. Here we provide the aspects of the theory most relevant to our present study.

In the framefork of the lattice description, space is divided into layers: spherical, cylindrical or planar, depending on the domain geometry. Each layer is further divided into lattice cells. Each cell is filled with one of the system

species (see Fig. 1). The lattice is scaled with a polymer segment size a, so all the lengths are measured in a units.

The Helmholtz free energy, A, of a multicomponent system with internal degrees of freedom includes three contributions:

$$\beta(A - A^*) = \beta(A_{\rm int} - A^*_{\rm int}) - \ln\frac{\Omega}{\Omega^*} + \beta(U - U^*)\,, \quad (1)$$

where $\beta = 1/k_{\rm B}T$, $k_{\rm B}$ being the Boltzmann constant and T the absolute temperature. $A_{\rm int}$ and U are the internal free energy and configurational energy, respectively, while $\ln(\Omega/\Omega^*)$ is the mixing conformational entropy. The quantities marked with an asterisk correspond to the reference pure amorphous system.

For a homogeneous mixture of the components, the three contributions are given by the following equations:

$$\beta A_{\rm int} = \sum_x \sum_A n_x r_{Ax} \sum_B P_{AB}\left[\beta U_{AB} + \ln\frac{P_{AB}}{g_{AB}}\right], \quad (2)$$

$$\ln\frac{\Omega}{\Omega^*} = -\sum_x n_x \ln\frac{n_x r_x}{L}\,, \quad (3)$$

$$\beta U = \frac{1}{2}\sum_x \sum_A \sum_{A'} \sum_B \sum_{B'} n_x r_{Ax} P_{AB} \chi_{BB'} P_{A'B'} \phi_{A'}\,. \quad (4)$$

Here r_{Ax} denotes the number of segments of type A (C, PO, EO or water) in component x ($(\mathrm{C})_k(\mathrm{PO})_n(\mathrm{EO})_m$ or water), r_x the total number of segments in component x ($k+n+m$ or 1), n_x the total number of molecules of type x, L the total number of lattice sites, ϕ_A the volume fraction of species A, and $\chi_{BB'}$ the Flory-Huggins interaction parameter between species A in state B and species A' in state B'. P_{AB} is the fraction of species A in state B. U_{AB} and g_{AB} are the internal energy and degeneration factor, respectively, of state B of species A; in the case of EO or PO these quantities describe the equilibrium between the polar and apolar states.

In a system with segregated components, a heterogeneity of species density is introduced in one direction, radial in the case of spherical or cylindrical lattice, and in the z-direction in the case of planar lattice. Within each layer, the Bragg-Williams approximation of random mixing is applied, and thus all sites in a layer are equivalent. Density distribution profiles are obtained as a function of layer number. The three contributions in equation (1) for heterogeneous system are written as follows:

$$\beta A_{\rm int} = \sum_i \sum_A n_{Ai} \sum_B P_{ABi}\left[\beta U_{AB} + \ln\frac{P_{ABi}}{g_{AB}}\right], \quad (5)$$

$$\ln\frac{\Omega}{\Omega^*} = -\sum_x \sum_c n_{xc} \ln\frac{n_{xc} r_x}{\omega_{xc}}\,, \quad (6)$$

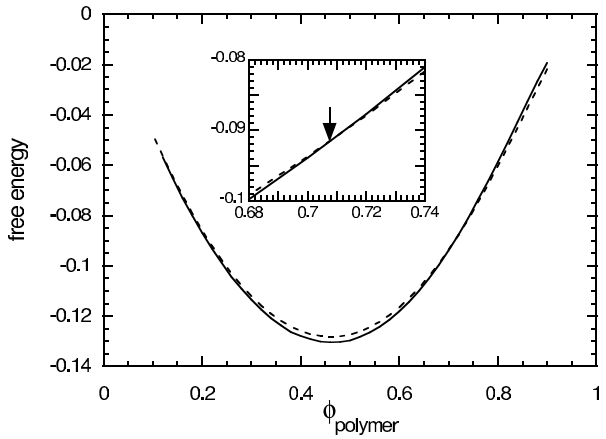

Fig. 2. Free energy for the hexagonal phase (solid curve) and the lamellar phase (dashed curve) as a function of polymer volume fraction at $T = 280$ K. The insert shows a range of $\phi_{\rm polymer}$ where two curves cross; an arrow points to the volume fraction where phase transition occurs.

where n_{xc} is the number of chains of component x in conformation c. w_{xc} is related to the degeneration of a conformation c of component x and it is given by equation (A.1.2) in reference [46]; and

$$\beta U = \frac{1}{2}\sum_i^M \sum_A \sum_{A'} \sum_B \sum_{B'} \phi_{Ai} P_{ABi} \chi_{BB'} \langle P_{A'B'i} \phi_{A'i}\rangle\,, \quad (7)$$

where L_i is the number of lattice sites in the layer i, A and A' run over all species and B and B' over all states. ϕ_{Ai} is the volume fraction of species A in layer i. $\langle ...\rangle$ indicates an average over the present and the two adjacent layers. M is the total number of the layers in the system corresponding to the domain size. At a given temperature and system composition the size of the domain is optimized.

In the calculations we use the difference between the free energy of a heterogeneous system of a certain structure given by the sum of contributions (5), (6) and (7), and the free energy of a homogeneous system given by the sum of (2), (3) and (4). The free-energy difference curves are obtained as a function of polymer volume fraction at a given temperature (see Fig. 2). Five ordered phases have been considered in this work: micellar cubic phase, I_1, hexagonal phase, H_1, lamellar phase L_α, reverse hexagonal phase, H_2, and reverse cubic (discrete) phase, I_2. In the temperature range 280–380 K of interest here only four of them, shown in Figure 3, are found stable. Phases of complicated topology are not considered in the present work, since we intend to focus on the most common and most stable structures.

To construct the phase diagram, phase boundaries have to be evaluated. For each temperature, two-phase regions can be determined by using the graphical double-tangent method (see Fig. 1 in Ref. [22]). Our calculations show that, throughout the whole temperature range considered here, the two-phase regions are narrow (see, for

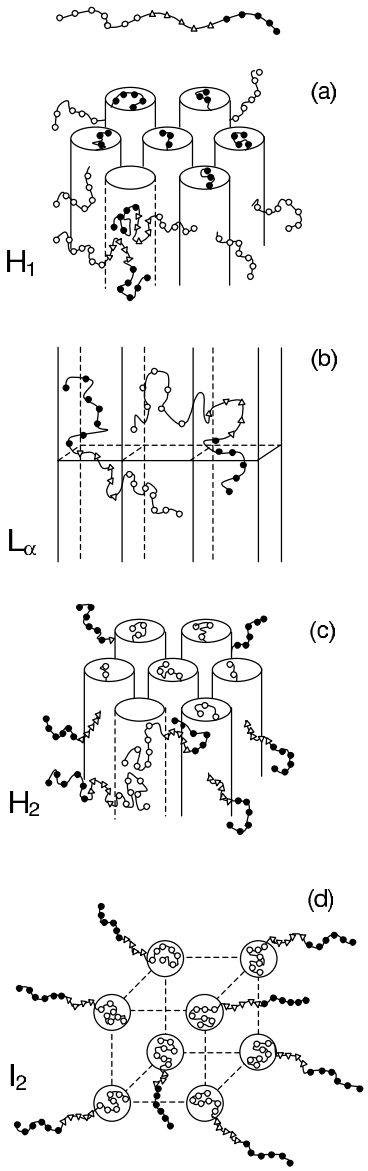

Fig. 3. Schematic illustration of different modes of self-organization of C-PO-EO triblock copolymer in water. Filled circles represent C-segments, open triangles represent PO-segments, and open circles represent EO-segments. Lyotropic liquid crystalline (ordered) phases are denoted as follows: (a) normal (water-continuous) hexagonal, H_1, (b) lamellar, L_α, (c) reverse (polymer-continuous) hexagonal, H_2, and (d) reverse micellar cubic, I_2.

example, the insert in Fig. 2). For simplicity, they are neglected, and we defined the location of a phase transition from the crossing of the free-energy curves (see insert in Fig. 2).

2.2 Species and interaction parameters

The general problem that we address in the present study is the phase behavior of ABC triblock copolymers in selective solvent. However, for reasons of practical interest we focus the problem to the specific case of aqueous solution. The considered molecule has the chemical structure $(C)_{14}(PO)_{12}(EO)_{17}$ and it is modeled as a triblock copolymer with 7 (-CH_2-CH_2-) segments, denoted 2C, 12 (-CH(CH_3)-CH_2-O-) segments, PO, and 17 (-CH_2-CH_2-O-) segments, EO. The modeled two-component system contains four species referred to as 2C-segments of alkyl block, PO-segments of poly(propylene oxide) block, EO-segments of poly(ethylene oxide) block, and W water molecules.

Table 1. Interaction parameters ($RT\chi_{BB'}$) of the theoretical model (energy in kJ mol^{-1})

	EO-P	EO-AP	PO-P	PO-AP	2C
W	0.6508[a]	5.568[a]	1.7[b]	8.5[b]	11.0
EO-P		1.266[a]	1.8[c]	3.0[c]	3.0
EO-AP			0.5[c]	−2.0[c]	0.0
PO-P				1.4[b]	0.0
PO-AP					0.0

([a]) From the fit to the experimental PEO/water phase diagram [43].
([b]) From the fit to the experimental PPO/water phase diagram [46].
([c]) From the fit to the experimental PEO/PPO/water phase diagram [20].

In the model, two states, polar P and apolar AP, are considered for each of the ethylene oxide and propylene oxide segments in order to account for the reverse temperature dependence of the solubility of PEO and PPO in water. The alkyl segments have a single state.

In the framework of the mean-field approach, all species experience a potential of mean force. Two contributions to the potential of mean force are considered in the theory, *viz.* those arising from i) hard-core interactions, and ii) short-range nearest-neighbors interactions described by Flory-Huggins χ-parameters.

The calculations for the model require some knowledge of the interaction χ-parameters between all pairs of species in different states. Parameters that describe the 10 binary interactions in a PO-, EO-, and W-containing system as well as the internal energy and degeneration of polar and apolar states were taken from previous works [20,43,46].

The χ-parameter for the water-ethylene interaction, W/2C, was taken in order to account for the high hydrophobicity of the alkyl block. It is experimentally observed [47] that at room temperature and $(C)_{14}(PO)_{12}(EO)_{17}$ block copolymer content $\approx 50\%$ the ordered hexagonal phase is stable. The value of $\chi_{W,2C}$ was tuned by performing the calculations at $T = 295$ K and $\phi_{polymer} = 0.5$. The $\chi_{W,2C}$ was chosen from the condition that the free energy of the normal hexagonal phase at given T and $\phi_{polymer}$ is lowest among all other ordered phases. As the first approximation, the binary interactions PO-P/2C, PO-AP/2C, and EO-AP/2C were considered athermal, and the EO-P/2C χ-parameter was taken equal to the EO-P/PO-AP χ-parameter. All interaction χ-parameters used in this work are compiled in Table 1.

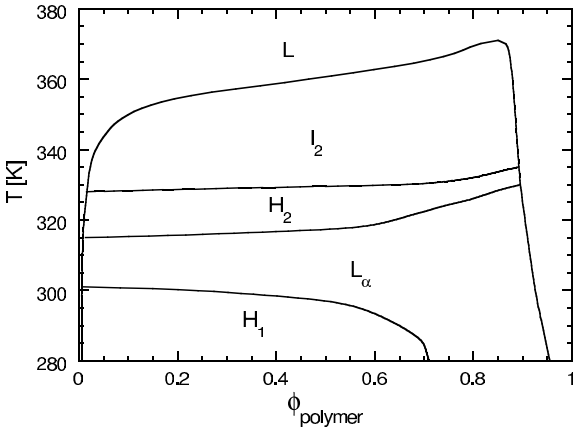

Fig. 4. Binary phase diagram in the coordinates: polymer volume fraction-temperature, for the system $(2C)_7(PO)_{12}(EO)_{17}$/water. The notation is the same as in Figure 2 with the addition that L denotes the disordered phase.

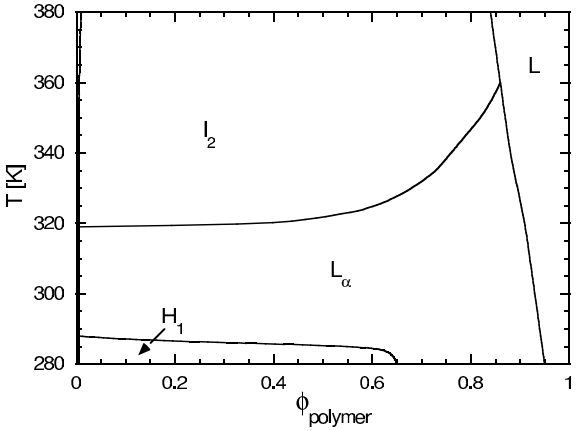

Fig. 5. Binary phase diagram in the coordinates: polymer volume fraction-temperature, for the system $(2C)_7(EO)_{17}$/water. The notation is the same as in Figure 4.

3 Results and discussion

3.1 Phase diagrams

In this section we present the calculated binary phase diagram of $(2C)_7(PO)_{12}(EO)_{17}$ in water in coordinates: polymer volume fraction-temperature. In the temperature range T = 280–380 K, the phase diagram exhibits four ordered phases: normal hexagonal, H_1, lamellar, L_α, reverse hexagonal, H_2, and reverse cubic I_2 phases (see Fig. 4). The disordered phase L in our model is defined as a homogeneous mixture of block copolymer and water. Other disordered structures, such as micellar solution, with spherical and/or cylindrical micelles, either normal or reverse, and two-phase regions with disordered water-rich and polymer-rich, phases have not been considered in the framework of the approach used here, because our present focus is on the formation and structure of the ordered phases.

The most striking feature of the phase diagram presented in Figure 4 is that of temperature-induced transitions between different ordered phases (thermotropic phase behavior). At polymer volume fractions ranging from very low to $\phi_{\text{polymer}} \approx 0.6$, as the temperature is increased, successive phase transitions take place from the hexagonal phase to lamellar phase, reverse hexagonal phase, reverse cubic phase, and disordered phase. In addition to the thermotropic behavior, in the temperature range T = 280–300 K an increase of the polymer volume fraction causes a transition from the hexagonal to the lamellar phase (lyotropic phase behavior).

Such phase organization is very different from the picture that has emerged for $(EO)_m(PO)_n(EO)_m$ block copolymers in water (see, *e.g.*, Refs. [21,22]). For these block copolymers the structural transitions are primarily induced by a change in the polymer volume fraction. The sequence of phase transitions with increasing polymer/solvent ratio is similar to that observed for block copolymers in melts (without selective solvent) upon varying the block composition [9,10].

In order to better understand the temperature effect on the phase behavior of $(2C)_7(PO)_{12}(EO)_{17}$ in water and to evaluate the contribution of each block on the phase behavior, we have examined the formation of ordered structures in the systems $(PO)_{12}(EO)_{17}$/water, $(2C)_7(PO)_{12}$/water and $(2C)_7(EO)_{17}$/water (*i.e.*, in addition to the ABC triblock copolymer, we considered the AB, AC, and BC diblock architectures).

By performing the model calculations, we have found that the diblock copolymers $(PO)_{12}(EO)_{17}$ in water do not form any micelles. Although it is known that the micellization of PPO-PEO diblocks occurs at lower temperature and lower polymer concentrations in the solution than the micellization of triblocks of the same block composition [48], the absolute block length plays indeed an important role in micellar stability. A decrease in the molecular weight of the blocks at constant relative PO/EO content shifts the critical micelle concentration (cmc) to higher concentrations and the critical micelle temperature (cmt) to higher temperatures [48,49]. Moreover, the temperature range over which micelles are stable is reduced as the polymer chain becomes shorter. Besides, one should note that the difference in hydrophobicity between EO and PO is only moderate, therefore the effective segment-segment interaction is weak. The addition of the alkyl block renders the self-assembly of the molecules entropically less costly and changes the hydrophobic/hydrophilic balance among the blocks.

Examination of the system $(2C)_7(PO)_{12}$/water shows that micelles are formed by $(2C)_7(PO)_{12}$ but do not organise in ordered phases in the considered temperature interval. On the basis of the approach that we use, we define the obtained structure as a solution of disordered micelles.

Liquid crystalline phases, however, are found for the system $(2C)_7(EO)_{17}$/water over the whole interval T = 280–380 K (Fig. 5). Such observation reflects the more prominent hydrophilic behavior of PEO relative to that of PPO (see Ref. [48]). The phase behavior of diblock copolymers $(2C)_7(EO)_{17}$ in water is thermotropic, similarly to what is found for the triblock copolymers

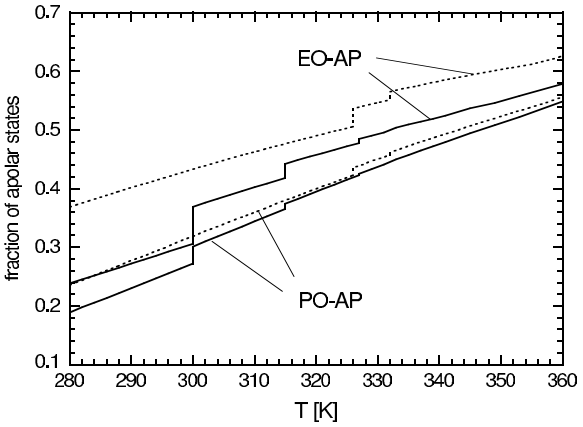

Fig. 6. Fraction of apolar states EO-AP and PO-AP in EO- and PO-block, respectively, as a function of temperature for the system $(2C)_7(PO)_{12}(EO)_{17}$/water at $\phi_{\text{polymer}} = 0.4$ (solid curves) and 0.8 (dotted curves).

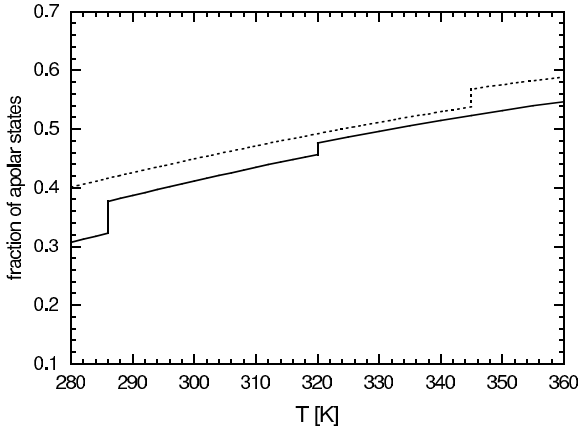

Fig. 7. Fraction of apolar states EO-AP in EO-block as a function of temperature for the system $(2C)_7(EO)_{17}$/water at $\phi_{\text{polymer}} = 0.4$ (solid curve) and 0.8 (dotted curve).

$(2C)_7(PO)_{12}(EO)_{17}$. From a comparison of the two phase diagrams shown in Figures 4 and 5, one can notice an increasing range of temperature stability of the lamellar and reverse cubic phases in the diblock/water system, and also a narrowing of the temperature range of hexagonal phase stability (the H_2 phase does not appear in the phase diagram shown in Fig. 5).

The basic temperature effect on the phase transitions in both di- and triblock copolymer/water systems can be explained within the two-state model formalism. The model allows the polymer segments to adopt an equilibrium state distribution that depends on the temperature and the polymer concentration. Figure 6 shows an increasing fraction of apolar states both for EO- and PO-segments in the corresponding blocks as the temperature is increased, calculated for the system $(2C)_7(PO)_{12}(EO)_{17}$/water. The fraction of apolar states increases with increasing temperature and with increasing polymer concentration. The discontinuities in the increasing function are due to the phase transition boundaries. In Figure 7 we present the fraction of apolar states in EO-block calculated for the system $(2C)_7(EO)_{17}$/water. The same temperature and concentration trends are observed for this system. However, the temperature dependence of the apolar EO-states fraction is stronger when PO-segments are present in the system (*cf.* Figs. 6 and 7).

The observed dependencies of the state distribution allow us to analyze the phase behavior of the binary $(2C)_7(PO)_{12}(EO)_{17}$/water and $(2C)_7(EO)_{17}$/water systems taking into account a given set of interaction χ-parameters (see Tab. 1). The 2C/water interaction parameter reflects the highly hydrophobic nature of alkyl block and correspondingly its location in a water-free part of the structural domain. The interaction between 2C- and PO-segment is athermal, whether PO-segments adopt a polar or an apolar state. The interaction between 2C-segment and EO-segment in the apolar state is athermal ($RT\chi_{\text{2C,EO-AP}} = 0$), whereas it is repulsive when the EO-segment is in the polar state ($RT\chi_{\text{2C,EO-P}} =$ 3 kJ mol^{-1}). At elevated temperatures the equilibrium state distribution shifts toward apolar states for both EO- and PO-segments. This means that the hydrophobic/hydrophilic difference between the 2C-block from one side and the PO- and EO-blocks from the other side becomes smaller. This leads to an effective renormalization of the copolymer composition: the hydrophobic part becomes longer with temperature and the hydrophilic part becomes correspondingly shorter, making reverse (polymer-continuous) structures more favorable. At the same time, the segregation between 2C- and EO-blocks becomes weaker and, therefore, concentration-induced (lyotropic) phase transitions vanish. At high polymer concentrations the effects are more pronounced and, as a result, no curved normal (water continuous) phases are observed there. In the diblock copolymer/water system a direct phase transition from lamellar to reverse cubic phase takes place. This is a result of two simultaneously developing effects: worsening of the solvent for EO-block and decreasing incompatibility between 2C- and EO-blocks.

3.2 Density profiles

In addition to phase behavior, other important features predicted from the theory are the volume fraction profiles of the polymer species 2C, PO, EO, and water W. To obtain real length units, we have used $a = 4$ Å for the length of a lattice cell, which has previously been shown to give reasonable agreement with experimental data [50]. The profiles in all ordered phases obtained for the $(2C)_7(PO)_{12}(EO)_{17}$/water system are presented in Figure 8 for two polymer volume fractions. They are obtained for different temperatures, and correspondingly different phases. In the normal hexagonal phase (Fig. 8a, e), the center of the cylinder is filled mostly with 2C-segments. ϕ_{2C} drops fast from a maximum value, whereas ϕ_{PO} increases with the distance from the center, and reaches its maximum at a distance where ϕ_{2C} has decreased sufficiently. The concentration of EO-segments

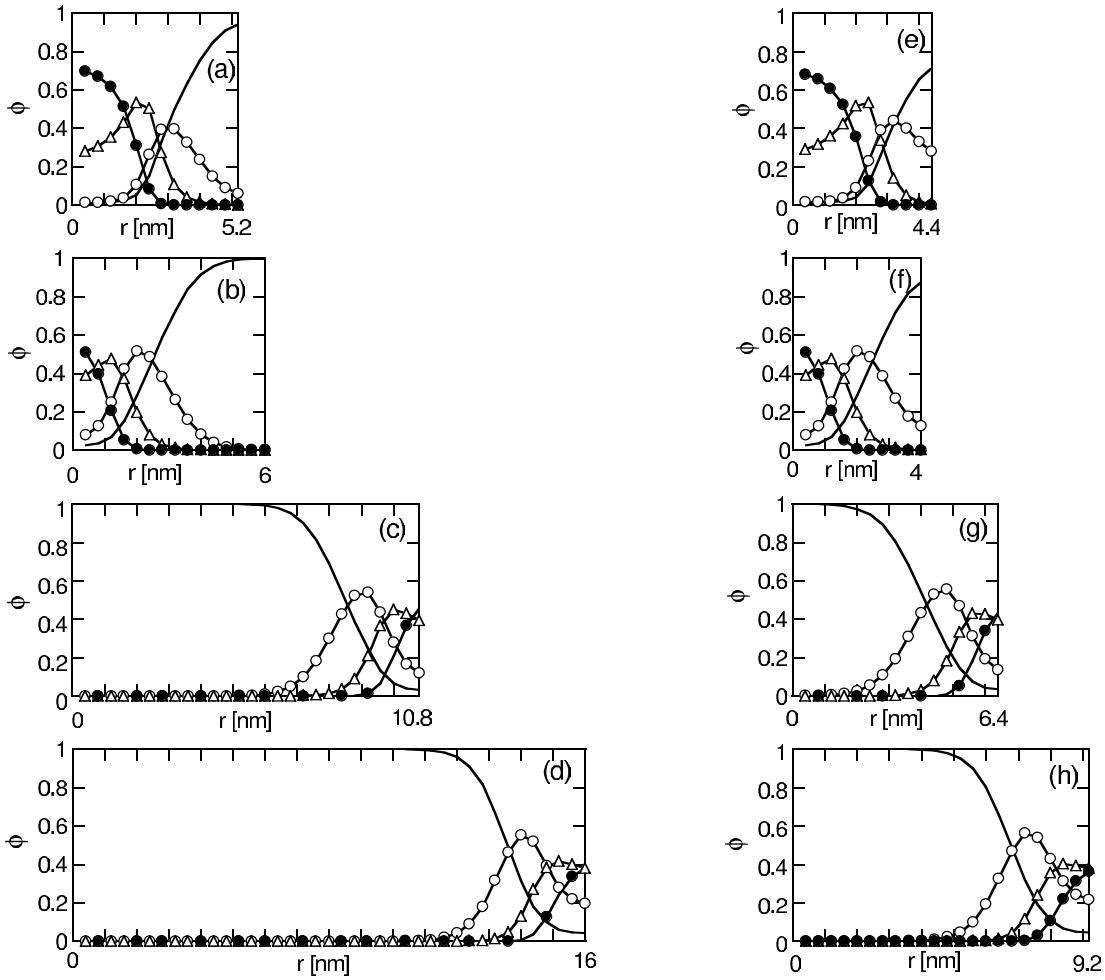

Fig. 8. 2C (filled circles), PO (open triangles), EO (open circles) and water (solid curve) volume fraction profiles for the $(2C)_7(PO)_{12}(EO)_{17}$/water system in the (a) normal hexagonal, (b) lamellar, (c) reverse hexagonal, and (d) reverse micellar cubic phases at the polymer volume fraction $\phi_{\text{polymer}} = 0.4$, and in the (e) normal hexagonal, (f) lamellar, (g) reverse hexagonal, and (h) reverse micellar cubic phases at the polymer volume fraction $\phi_{\text{polymer}} = 0.6$. $T = 290$ K for the normal hexagonal, $T = 310$ K for the lamellar, $T = 320$ K for the reverse hexagonal, and $T = 350$ K for the reverse micellar cubic phase. Note that the r-scale varies due to the different optimum domain spacings.

is very low in the center of the cylinder and exhibits a maximum far away from it. From such profiles one can conclude that the domain has a "triple-layer" structure, with a 2C-rich center, PO-rich intermediate layer, and EO-rich periphery. In the center of the domain $\phi_{2C} + \phi_{PO} \approx 1$, thus, no water or EO-segments penetrate the region where 2C- and PO-segments are located.

The main features of the profiles for the lamellar phase (Fig. 8 b, f) are the same as for the normal hexagonal phase, except for the location of the ϕ_{EO} peak. Since at higher temperatures the EO-block becomes more hydrophobic, it tries to reduce its contact with water and stay closer to the center of the domain. At the same time, the separation between 2C- and PO-block as well as between 2C- and EO-block decreases, and some water penetrates the core accompanying the EO-segments.

The density profiles for the reverse hexagonal and for the reverse cubic phases are shown in Figures 8c, g and 8d, h, respectively. The interior of the assembly, cylindrical or spherical, is filled with water, and the maxima of ϕ_{PO} and ϕ_C are located at the periphery. EO-segments form a layer outside the water core. From a comparison of Figures 8a–d one can conclude that the domain spacing increases as the temperature is increased. This fact is consistent with the increased hydrophobicity of the EO- and PO-blocks as it is inferred from the increase in apolar states fraction predicted by the model. It is also seen that for reverse structures the domain grows due to significant solvation of EO-block. The mixing of the blocks is increased reflecting the fact of decreasing (C)/(EO) incompatibility.

In Figures 8e–h the profiles are shown for the higher polymer volume fraction ($\phi_{\text{polymer}} = 0.6$). One can note that the profiles are qualitatively the same for both polymer concentrations. However, a difference in the domain spacing is noticeable. The size of the domain is smaller for the higher polymer concentration and it increases slowly with increasing temperature; it even decreases when passing from the normal hexagonal to the lamellar phase

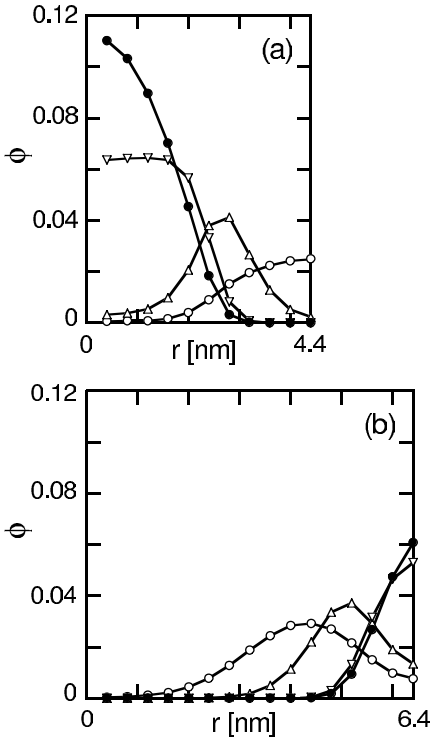

Fig. 9. Free EO-end (open circles) and 2C-end (filled circles) and EO-PO-junction (open up triangles) and PO-2C-junction (open down triangles) distributions for the $(2C)_7(PO)_{12}(EO)_{17}$/water system in the (a) normal hexagonal phase at the temperature $T = 290$ K, and (b) reverse hexagonal phase at the temperature $T = 320$ K. Polymer volume fraction $\phi_{\text{polymer}} = 0.6$.

(*cf.* Figs. 8e and f). (The domain spacing behavior is considered in more detail in Sect. 3.4.)

3.3 End and junction distributions

The lattice theory also provides volume fraction profiles of segments of given rank. Figure 9 shows the two end and the two junction distributions for the $(2C)_7(PO)_{12}(EO)_{17}$/water system in the normal and reverse hexagonal phases at $\phi_{\text{polymer}} = 0.6$. As one can see from a comparison of Figures 9a and 8e, in the normal hexagonal phase the 2C-end distribution closely follows the distribution of all segments, indicating that the 2C-blocks are not stretched in the core of the domain. The EO-end distribution is broad and without maximum, which means that the EO-blocks are not stretched in the corona. The distribution of the EO-PO-junction has a well-pronounced maximum that is identified with the hydrophobic core-hydrophilic corona interface. The PO-2C-junction distribution is uniform in the region where the PO- and 2C-segments are located (*cf.* Fig. 8e), therefore, we can conclude that PO- and 2C-segments are only slightly separated. In the reverse hexagonal phase (see Fig. 9b), the end and junction distributions follow the distribution of the segments (*cf.* Fig. 8g), suggesting

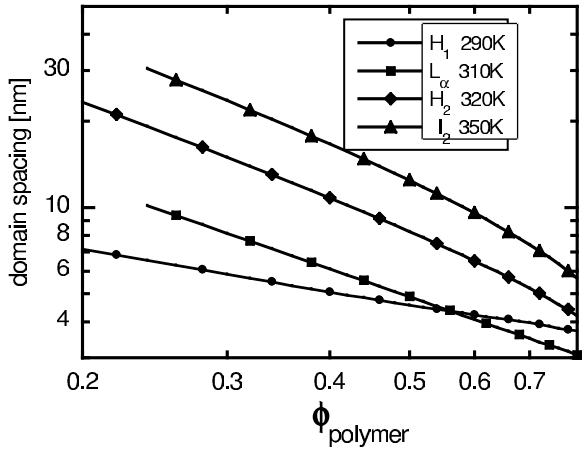

Fig. 10. Domain spacing as a function of polymer volume fraction in double logarithmic scale for the $(2C)_7(PO)_{12}(EO)_{17}$/water system in the different ordered phases and correspondingly different temperatures (indicated in the figure).

the existence of a polymer free center, and an interface between an EO-rich layer and a 2C- and PO-rich periphery with strong mixing of PO- and 2C-segments.

3.4 Domain spacing

Scattering measurements (SAXS or SANS) are often used to characterize ordered phases in block copolymer-selective solvent systems [13,51,52]. The magnitude of the principal scattering vector provides a measure of the domain spacing. Domain spacing information can also be obtained from the mean-field theory used here. Figure 10 displays the calculated domain spacing in the ordered phases of the $(2C)_7(PO)_{12}(EO)_{17}$/water system as a function of polymer volume fraction at different temperatures.

The domain size within a given ordered phase decreases with increasing polymer concentration. There are two factors that can explain such behavior: i) the amount of water per block copolymer forming the domain decreases resulting in deswelling of the solvated blocks; ii) the fraction of the apolar states of both EO- and PO-segments is larger at higher polymer concentration (see Fig. 6), so that the effective EO/W and PO/W interactions are more hydrophobic, therefore the interfacial area shrinks to reduce unfavorable contacts between hydrophobic segments and water. The L_α, H_2, and I_2 phases exhibit stronger ϕ_{polymer} dependence than the H_1 phase. In the normal hexagonal phase at $\phi_{\text{polymer}} > 0.55$, the size of the domain becomes bigger than in the lamellar phase at the same polymer content (see also density profiles in Fig. 8).

In Figure 11 the calculated domain spacing is plotted as a function of temperature at $\phi_{\text{polymer}} = 0.4$ and 0.8. The discontinuities are due to the phase transition boundaries. The observation that at higher polymer concentration the domains become smaller is consistent with the

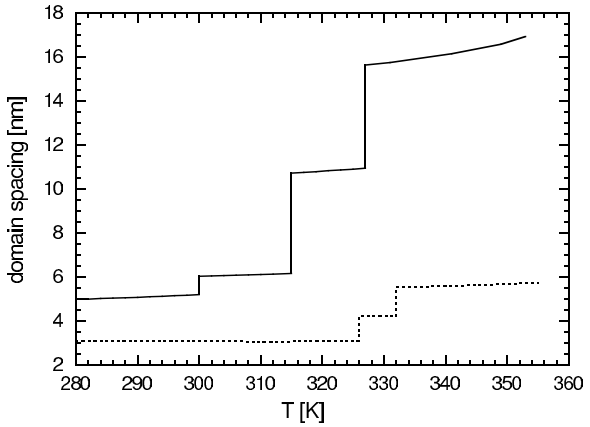

Fig. 11. Domain spacing as a function of temperature for the $(2C)_7(PO)_{12}(EO)_{17}$/water system in the different ordered phases at $\phi_{\text{polymer}} = 0.4$ (solid curve) and 0.8 (dotted curve).

trends shown in Figure 10. Moreover, the temperature dependence is weaker for the higher ϕ_{polymer}. This can be explained by the following argument: although the fraction of the apolar states increases with temperature proportionally for low and high ϕ_{polymer} (see Fig. 6), the fact that the total amount of the apolar states is larger for higher polymer concentration plays an important role. An assembly with a larger fraction of hydrophobic segments has a smaller interface than an assembly with a smaller fraction. Increasing temperature causes an effective worsening of the solvent that leads to a shrinking of the interface. A larger interfacial area decreases faster than a smaller one.

4 Conclusions

In the present paper we have shown that the mean-field lattice theory is capable of predicting the formation and structure of ordered phases formed by an ABC triblock copolymer in a selective solvent. To our knowledge, there are no other theoretical or experimental studies of such systems. The phase diagram for the system $(2C)_7(PO)_{12}(EO)_{17}$/water is obtained as a function of polymer concentration and temperature using the interaction parameters known from previous works (between all pairs in EO-, PO-, W-containing system) and estimated in this work (2C between EO, PO, and W).

The calculated phase diagram exhibits four ordered phases, namely H_1, L_α, H_2 and I_2, and a disordered phase L. At sufficiently low temperatures, a transition from H_1 to L_α caused by increasing polymer concentration occurs. Such transition is typical for many PEO/PPO block copolymers. A temperature-induced sequence of phase transitions $H_1 \rightarrow L_\alpha \rightarrow H_2 \rightarrow I_2$ over a wide range of polymer volume fraction is a new observation for the ABC triblock copolymer considered in the present study. The thermotropic behavior results from the fact that the water interaction with EO- and PO-segments has a strong temperature and concentration dependence. Elevated temperatures worsen the solvency conditions for EO- and PO-blocks and decrease the incompatibility between 2C- and EO-blocks. The temperature effect becomes stronger as the polymer concentration is increased.

In the domain structure one can distinguish three layers, 2C-rich, PO-rich, and EO-rich, respectively. The blocks forming the domain are not stretched. With increasing temperature the structure reverses from solvent-continuous to polymer-continuous and the size of the domain increases.

The present work opens fields for future studies. Experimental verification of the predicted phase behavior at the bicomponent $(2C)_7(PO)_{12}(EO)_{17}$/water system is in progress. Moreover, in order to achieve better tuning of the interaction χ-parameters we are working to determine the phase diagrams for $(2C)_7(PO)_{12}(EO)_m$ block copolymers in water for different length of $(EO)_m$-block, both experimentally and by model calculations.

PA acknowledges The Dow Chemical Co. for a grant that funded this research.

References

1. I. Hamley, *The Physics of Block Copolymers* (Oxford University Press, Oxford, 1998)
2. F.J.B. Callejia, Z. Roslaniec (Editors), *Block Copolymers* (Marcel Dekker, New York, 2000)
3. L. Leibler, Macromolecules **13**, 1602 (1980)
4. A.N. Semenov, Sov. Phys. JETP **61**, 733 (1985)
5. G.H. Fredrickson, E. Helfand, J. Chem. Phys. **87**, 697 (1987)
6. M.W. Matsen, F.S. Bates, Macromolecules **29**, 1091 (1996)
7. F.S. Bates, M.F. Schulz, A.K. Khandpur, S. Förster, J.H. Rosedale, K. Almdal, K. Mortensen, Faraday Discuss. **98**, 7 (1994)
8. G.H. Fredrickson, F.S. Bates, Annu. Rev. Mater. Sci. **26**, 501 (1996)
9. G. Floudas, B. Vazaiou, F. Schipper, R. Ulrich, U. Wiesner, H. Iatrou, N. Hadjichristidis, Macromolecules **34**, 2947 (2001)
10. S. Förster, B. Berton, H.-P. Hentze, E. Krämer, M. Antonietti, P. Lindner, Macromolecules **34**, 4610 (2001)
11. P. Alexandridis, D. Zhou, A. Khan, Langmuir **12**, 2690 (1996)
12. P. Alexandridis, Macromolecules **31**, 6935 (1998)
13. P. Alexandridis, U. Olsson, B. Lindman, Langmuir **14**, 2627 (1998)
14. K.J. Hanley, T.P. Lodge, C.-I. Huang, Macromolecules **33**, 5918 (2000)
15. N.R. Washburn, T.P. Lodge, F.S. Bates, J. Phys. Chem. **104**, 6987 (2000)
16. P. Alexandridis, Curr. Opin. Colloid Interface Sci. **2**, 478 (1997)
17. P. Alexandridis, R.J. Spontak, Curr. Opin. Colloid Interface Sci. **4**, 130 (1999)
18. R.J. Spontak, P. Alexandridis, Curr. Opin. Colloid Interface Sci. **4**, 140 (1999)
19. P. Alexandridis, B. Lindman (Editors), *Amphiphilic Block Copolymers: Self-Assembly and Applications* (Elsevier Science B. V., Amsterdam, 2000)

20. M. Malmsten, P. Linse, K.-W. Zhang, Macromolecules **26**, 2905 (1993)
21. J. Noolandi, A.-C. Shi, P. Linse, Macromolecules **29**, 5907 (1996)
22. M. Svensson, P. Alexandridis, P. Linse, Macromolecules **32**, 637 (1999)
23. G. Wanka, H. Hoffman, W. Ulbricht, Macromolecules **27**, 4145 (1994)
24. X.H. Yan, F.T. Liu, Z. Li, G.J. Liu, Macromolecules **34**, 9112 (2001)
25. H. Schmalz, A. Boker, R. Lange, G. Krausch, V. Abetz, Macromolecules **34**, 8720 (2001)
26. M.L. Arnal, V. Balsamo, F. Lopez-Carrasquero, J. Contreras, M. Carrillo, H. Schmalz, V. Abetz, E. Laredo, A.J. Muller, Macromolecules **34**, 7973 (2001)
27. A. Boker, A.H.E. Muller, G. Krausch, Macromolecules **34**, 7477 (2001)
28. C.S. Patrickios, C. Forder, S.P. Armes, N.C. Billingham, J. Polym. Sci., Polym. Chem. **35**, 1181 (1997)
29. J. Kriz, B. Masar, J. Prestil, Z. Tuzar, H. Pospisil, D. Doskocilova, Macromolecules **31**, 41 (1998)
30. G.-E. Yu, A. Eisenberg, Macromolecules **31**, 5546 (1998)
31. M. Sugiyama, T.A. Shefelbine, M.E. Vigild, F.S. Bates, J. Phys. Chem. B **105**, 12448 (2001)
32. T.S. Bailey, H.D. Pham, F.S. Bates, Macromolecules **34**, 6994 (2001)
33. V. Abetz, R. Stadler, L. Leibler, Polym. Bull. **37**, 135 (1996)
34. V. Abetz, R. Stadler, Macromol. Symp. **113**, 19 (1997)
35. U. Breiner, U. Krappe, V. Abetz, R. Stadler, Macromol. Chem. Phys. **198**, 1051 (1997)
36. I. Erukhimovich, V. Abetz, R. Stadler, Macromolecules **30**, 7435 (1997)
37. W. Zheng, Z.-G. Wang, Macromolecules **28**, 7215 (1995)
38. M.W. Matsen, M. Schick, Curr. Opin. Colloid Interface Sci. **1**, 329 (1996)
39. J.M.H.M. Scheutjens, G.J. Fleer, J. Phys. Chem. **83**, 1619 (1979); **84**, 178 (1980)
40. F.A.M. Leermakers, J.M.H.M. Scheutjens, R.J. Gaylord, Polymer **25**, 1577 (1984)
41. F.A.M. Leermakers, J.M.H.M. Scheutjens, J. Chem. Phys. **89**, 3264 (1988)
42. M.R. Böhmer, O.A. Evers, J.M.H.M. Scheutjens, Macromolecules **23**, 2288 (1990)
43. G. Karlström, J. Phys. Chem. **89**, 4962 (1985)
44. M. Anderson, G. Karlström, J. Phys. Chem. **89**, 4957 (1985)
45. M. Björling, P. Linse, G. Karlström, J. Phys. Chem. **94**, 471 (1990)
46. P. Linse, M. Björling, Macromolecules **24**, 6700 (1991)
47. P. Alexandridis *et al.*, unpublished results
48. P. Linse, Macromolecules **26**, 4437 (1993)
49. P. Alexandridis, J.F. Holzwarth, T.A. Hatton, Macromolecules **27**, 2414 (1994)
50. P. Linse, T.A. Hatton, Langmuir **13**, 4066 (1997)
51. P. Alexandridis, R. Ivanova, B. Lindman, Langmuir **16**, 3676 (2000)
52. P. Holmqvist, P. Alexandridis, B. Lindman, J. Phys. Chem. B **102**, 1149 (1998)